Journal of Power Sources 196 (2011) 9702–9707

Contents lists available at ScienceDirect

Journal of Power Sources

journal homepage: www.elsevier.com/locate/jpowsour

$xLi_2MnO_3\cdot(1-x)LiMO_2$ blended with $LiFePO_4$ to achieve high energy density and pulse power capability

Kevin G. Gallagher[a,*], Sun-Ho Kang[a], Sei Ung Park[b], Soo Young Han[b]

[a] Chemical Sciences and Engineering Division, Argonne National Laboratory, 9700 South Cass Ave, Argonne, IL 60439, United States
[b] Hanwha Chemical Research & Development Center, 6 Shinsung Dong, Yuseong Gu, Daejon 305-804, Republic of Korea

ARTICLE INFO

Article history:
Received 6 June 2011
Received in revised form 14 July 2011
Accepted 15 July 2011
Available online 22 July 2011

Keywords:
Lithium rich
Iron phosphate
Blended electrode
Lithium-ion battery

ABSTRACT

A lithium-ion positive electrode is proposed that contains both high energy density and efficient pulse power capability, even at low state-of-charge (SOC). The pulse power capability at low SOC is attractive for applications, such as plug-in hybrid electric vehicles (PHEVs), which require pulse power operation over the entire useable SOC window. A lithium- and manganese-rich transition-metal layered-oxide (LMR-NMC), also classified as a layered–layered oxide material, is blended with a lithium iron phosphate (LFP) to achieve a potentially low-cost, high-performance electrode. The LMR-NMC material provides high energy by delivering cathode material gravimetric energy densities greater than 890 Wh kg^{-1}. The pulse power capability of this material at low SOC is greatly improved by incorporating a modest quantity of LFP. The LFP serves as an internal redox couple to charge and discharge the more rate-limited LMR-NMC material at moderate to low SOCs.

1. Introduction

Being an attractive means of efficient electrochemical energy storage, lithium-ion (Li-ion) batteries are widely implemented in the consumer electronics industry, currently being developed to electrify automotive drivetrains, and actively considered for integration into other applications [1,2]. Electrification of the transportation sector offers many potential advantages such as reducing petroleum consumption levels and lowering green-house gas emissions. However, to enable the widespread adoption of this battery chemistry into the transportation sector and other new applications, the battery cost must be lowered while lifetime and safety performance are simultaneously improved. This is especially true for applications where larger batteries are required, such as in battery electric vehicles (BEVs) and plug-in electric vehicles (PHEVs).

Reducing the positive electrode material cost has been shown to significantly lower the cost of a battery [3,4]. Current Li-ion positive electrodes are largely based on transition-metal layered-oxide materials, $LiMO_2$ (M = Ni, Co, Mn, Al, etc.). $LiCoO_2$, $LiNi_{0.80}Co_{0.15}Al_{0.05}O_2$, and $Li_{1+x}(Ni_{1/3}Co_{1/3}Mn_{1/3})_{1-x}O_2$ are examples of commercially available positive electrode materials providing excellent performance at a relatively high cost. The high cost is generally a function of the cobalt and nickel content; therefore, the cost of a positive electrode material may be decreased by increasing the manganese content while simultaneously reducing that of cobalt and nickel. Lithium- and manganese-rich transition metal layered-oxides (LMR-NMCs) [5–7] show great promise as positive electrode materials for Li-ion batteries as they can deliver significantly higher energy density than the aforementioned commercially available layered-oxides at a potentially lower cost (in terms of \$ kg^{-1} and \$ Wh^{-1}). The increased lithium and manganese content promotes the formation of Li_2MnO_3 or Li_2MnO_3-like regions in the transition-metal layer of the metal oxide [5,6]. Activation of the Li_2MnO_3 component, by charging to potentials higher than 4.4 V vs. Li^+/Li, results in a cathode material with reversible capacity greater than 200 mAh g^{-1}. A synergistic advance is being made with the implementation of LMR-NMC in that one may achieve higher energy density and lower cost through the same pathway.

Transportation applications (e.g. PHEVs and EVs) require not only high energy density but also moderate rate- and pulse-power capability over the full state-of-charge (SOC) range from which the useable energy is consumed. To date, however, the LMR-NMC materials have shown only modest rate capability. We expect improved LMR-NMC materials to be developed or engineered to have lower impedance than the currently widely communicated oxides. Some initial promising results have been communicated [8–11]. Nevertheless, the impedance at low SOC will most likely remain higher than desired due to the inherent nature of layered-oxides [12–15]. One of the solutions to achieve both the energy and power from the LMR-NMC cathode would be to physically blend LMR-NMC with an additional cathode material having good pulse-power characteristics.

* Corresponding author. Tel.: +1 630 252 4473; fax: +1 630 252 4176.
E-mail address: kevin.gallagher@anl.gov (K.G. Gallagher).

0378-7753/$ – see front matter © 2011 Elsevier B.V. All rights reserved.
doi:10.1016/j.jpowsour.2011.07.054

Literature has several examples of positive electrodes composed of blended active materials to meet different design requirements such as reduced irreversible capacity, increased life, SOC monitoring, rate performance, and others [16–22]. The blending of layered-oxides with spinel materials has been reported to a great extent [17,18,23,24]. The measurement and modeling of the improved rate capability of primary batteries from blended cathodes has also been communicated [21,25]. Albertus et al. modeled the discharge curves of a layered- and spinel oxides physical mixture [24]. However, the pulse behavior of blended cathodes has not been discussed in great detail even though pulse capability of a battery is a requirement for any power systems used in for automobile transport [26]. The purpose of this work is to present a system with enhanced pulse power capability over a wide SOC range while analyzing the electrochemical processes underlying the performance improvement.

The olivine material, $LiFePO_4$ (LFP), has been studied extensively and shown to have excellent rate capability when the particles are sufficiently small, coated with carbon, and free from blockage in the 1D lithium-ion transport channels [27–30]. Furthermore, the olivine compound contains much stronger bonds to the oxygen atoms than other oxide materials resulting in a very safe and stable cathode [30]. The reversible capacity of LFP is ~160 mAh g^{-1} (170 mAh g^{-1} theoretical) along a voltage plateau near 3.4 V vs. Li^+/Li. Because of the relatively low discharge voltage and poor packing density of nanoparticles, LFP may not be an attractive cathode material, as it is, for energy applications. However, the excellent rate capability at ≤3.4 V vs. Li^+/Li coupled with the superb structural stability makes LFP an ideal candidate to blend with the LMR-NMC materials to improve the positive electrode impedance. The flat voltage profile of LFP at low cell potentials for the blended electrode may also serve as an indicator to the battery that the system is near the end of discharge. What is more, the raw materials of LFP are earth abundant and thus low in cost. If processing costs are reduced in the future, LFP has the possibility of being a low-cost component of the battery. The blending of LFP with LMR-NMC has been reported in literature [22]. The authors found little synergy between the two materials they studied, although this may relate to the specific materials used in their work and that the effort was focused on the arrangement of the materials on current collector. The objective of this study is to evaluate if the blending of the high-energy LMR-NMC material with the high-power LFP material will result in a system that offers both high energy density, pulse power capability, and potentially low cost.

2. Experimental

2.1. Electrode materials

Based upon extensive previous work, mildly-fluorinated $0.5Li_2MnO_3{\cdot}0.5LiNi_{0.44}Mn_{0.31}Co_{0.25}O_2$ was selected as the LMR-NMC material for this study [9,31–33], which will be referred to as ANL-NMC hereafter. Synthesis of the ANL-NMC material is well described in literature [9,32–34].

The LFP was synthesized by hydrothermal method in supercritical water [35] at Hanwha Chemical supercritical hydrothermal pilot plant. The secondary particles have a D50 value of 10 μm, composed of primary particles with mean particle size of 250 nm. The specific surface area measured by the BET method is 15 m^2 g^{-1}. The residual carbon content in the LFP powder was measured to be 2.2 wt% of total mass.

2.2. Blending

The ratio of ANL-NMC and LFP in the mixture is important to meet both power and energy requirements. A simple calculation can be made to guide us in deciding the proper ratio of the two electrode materials for the blended cathode. If we assume the LFP material is the only active component at low SOC, we may estimate the approximate C-rate required from LFP to provide all the demanded current as a function of weight percent of LFP added. In this estimation, 150 and 200 mAh g^{-1} were used as the 1C rate capacities for LFP and ANL-NMC, respectively [9]. The result of this simple calculation is given in Fig. 1, showing a cathode based on 20 wt% LFP and 80 wt% ANL-NMC is a reasonable balance between rate capability and LFP content. For a 3C pulse based on the total capacity of the electrode, the LFP will have to deliver energy at a 19C rate assuming only the LFP participates. Compared to a graphite/ANL-NMC cell, the theoretical active material energy density is calculated to reduce only by 6.5% from the inclusion of 20 wt% LFP. We chose this composition for the blended electrode studied in this work. Optimization of the electrode would obviously require testing of various compositions; however, the goal of this work is not to present an optimization study but to demonstrate the feasibility of the concept for blending of these two materials.

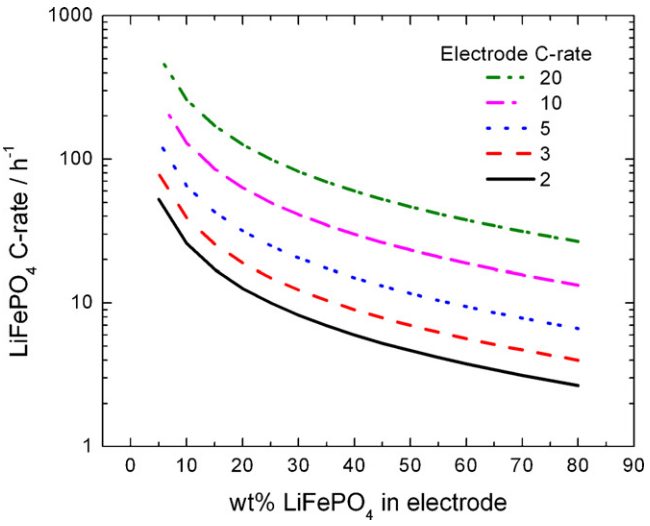

Fig. 1. Relationship between C-rate based on total battery capacity and C-rate for LFP particles assuming the LFP carries all of the current demanded. For a battery C-rate of $3C_{total}$, the LFP in a 20 wt% blend must discharge at a $19C_{LFP}$ rate to carry the entire current load.

2.3. Electrochemistry

The electrochemistry of the positive electrode materials, ANL-NMC, LFP, and ANL-NMC/LFP blended electrode, was evaluated in a 2032 coin cell format. The electrolyte used was 1.2 M $LiPF_6$ in a 3:7 mixture (by weight) of ethylene carbonate and ethylmethyl carbonate. The ANL-NMC and ANL-NMC/LFP blended positive electrodes were fabricated by mixing 82 wt% active material, 8 wt% carbon black (Super P Li, Timcal), and 10 wt% polyvinylidene fluoride (PVdF) binder (Kynar, Elf-Atochem) in N-methyl-2-pyrrolidone (NMP) solvent (Sigma–Aldrich, anhydrous, 99.5%) and spreading the slurry onto a 20-μm thick aluminum foil current collector with a doctor blade. The resulting laminate was dried in a 70 °C oven before being calendered to approximately 35% electrode porosity. The ANL-NMC and ANL-NMC/LFP positive electrode loading was typically around 3.75–4.25 mg cm^{-2}. The LFP electrode consisted of 90 wt% active material, 5 wt% of carbon, and 5 wt% PVdF binder with an active material loading of 9.54 mg cm^{-2}. The negative electrode was lithium foil (FMC Corporation) for the half-cell configuration and MAG-10 graphite (Hitachi Powdered Metals Co. Ltd.) for the full cell configuration, the latter of which was produced by a commercial battery manufacturer. The MAG-10

graphite electrode has a loading of 4.9 mg cm^{-2} or 1.6 mAh cm^{-2} at 15 mA g^{-1}. The full cells were designed with an excess of negative electrode capacity to accommodate the low first cycle efficiency of the ANL-NMC material used in this work and to prevent any lithium plating during charge pulsing. The target negative-to-positive first-cycle capacity ratio was 1.2. The separator was a polypropylene–polyethylene–polypropylene tri-layer membrane (Celgard 2325). The coin cells were assembled in a helium-filled glove box with less than 10 ppm H_2O and O_2. The laminates and separators were dried in a vacuum oven at 70 °C before being transferred to the glove box. The testing of the coin cells was performed at room temperature (~22 °C) with a MACCOR series 2000 cycler. Two formation cycles of 2–4.6 V at 15 mA g^{-1} with a 3-h trickle charge at 4.6 V were preformed before any additional testing.

Area-specific impedance (ASI) values were calculated based on the voltage response of a full-cell to a 10-s current pulse. The cells were charge to 4.4 V at a C/3 rate and then held at 4.4 V until the current decreased to C/30. Then 5% of the C/3 rated capacity was removed. The current was then interrupted and the cell voltage was allowed to relax for 60 min. The cell was then subjected to a 3C discharge pulse for 10 s. After an additional 60 min open-circuit rest, a 3C charge pulse was made for 10 s. The cell then rests for a final 60-min period before the galvanostatic cycle was repeated additional 18 times.

3. Results and discussion

The first-cycle charge and discharge curves for separate half cells containing ANL-NMC and LFP in 4.6–2.0 V at currents of 15 and 11 mA g^{-1}, respectively, are compared in Fig. 2a. The dramatically different capacities and voltages of the two positive electrode materials are obvious in this graphical format. The voltage plateau of LFP is near 3.40 V during the discharge and 3.46 V during the charge. The specific capacity of the first discharge is 165 mAh g^{-1} for LFP versus 230 mAh g^{-1} for ANL-NMC. The higher capacity for ANL-NMC also comes at a higher average voltage than the LFP material. Fig. 2b displays the voltage profiles during the 1st and 4th cycles of a blended electrode composed of 80 wt% ANL-NMC and 20 wt% LFP, cycled between 4.6 and 2.0 V at 15 mA g^{-1} with a trickle charge for 3 h at 4.6 V. The voltage plateau at 4.4 V from the Li_2MnO_3 activation, as well as the voltage plateau at 3.46 V from the LFP component, is clearly visible during the first charge. The first cycle efficiency of the blended electrode (79.4%) is slightly higher than that of the ANL-NMC electrode (76.6%), which is attributed to the near 100% cycle efficiency of LFP, as shown in Fig. 2a.

Fig. 3 shows capacity variations against cycle number of the lithium cells shown in Fig. 2. All of the three lithium cells maintain their capacity over the entire test. The LFP electrode shows the most stable cycling performance, albeit it shows the lowest average coulombic cycle efficiency of 98.1%. The ANL-NMC and blended electrodes have average cycling efficiency of 98.7 and 99.6% respectively, excluding the first activation cycle. The LFP electrode delivers a stable discharge capacity of 165 mAh g^{-1} over the whole cycles, showing the superior structural stability of LFP over 100% SOC cycles.

Fig. 4 compares the rate capability of the ANL-NMC to the blended electrode. The capacity of the blended electrode is only slightly compromised at current densities lower than 75 mA g^{-1} (~C/3). The inset in Fig. 4 shows the average voltage at which the energy is delivered to be essentially the same at 75 mA g^{-1}. At current densities higher than 75 mA g^{-1}, the blended electrode shows better capacity retention; the capacity of the blended electrode is ~40% higher than that of ANL-NMC at the discharge current density of 1.5 A g^{-1}. The improved rate capability is a result of the facile intercalation of Li-ions in the LFP. The residual carbon on the LFP

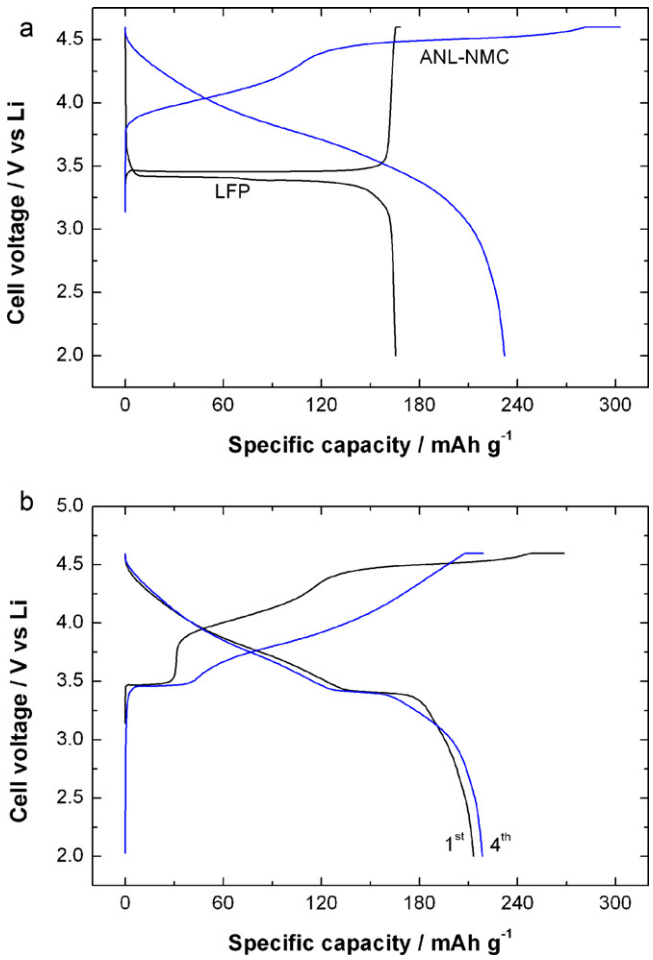

Fig. 2. (a) First cycle for LFP and ANL-NMC separately and (b) first and fourth cycle for 20 wt% LFP in half cell configuration.

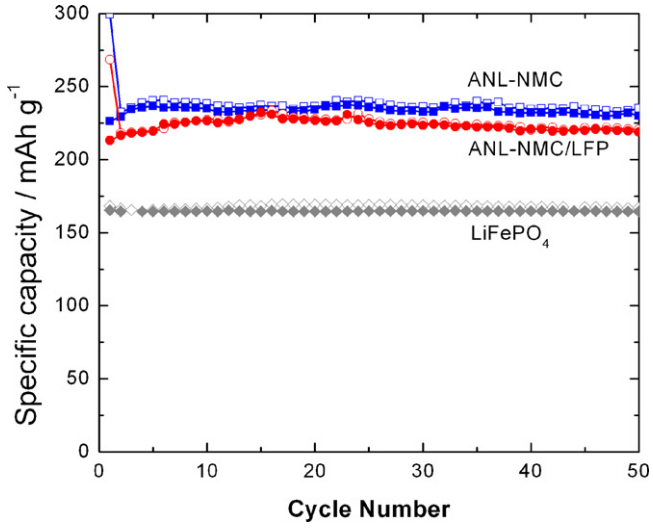

Fig. 3. Half cell cycling results of LFP, ANL-NMC, and 80 wt% ANL-NMC 20 wt% LFP.

particles may also serve to increase the overall electronic conductivity of the electrode. Future optimization studies could look to reduce the amount of conductive additive mixed into the porous electrode, further improving the power and energy density [36].

The pulse discharge and charge behavior of secondary batteries is often characterized by an empirical parameter called the area

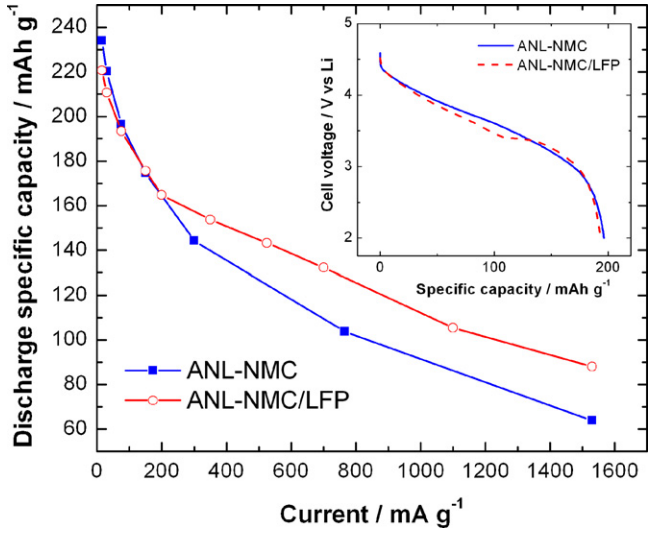

Fig. 4. Rate capability for half cells of ANL-NMC and a blended active material configuration of 20 wt% LFP and 80 wt% ANL-NMC. (Inset) C/3 discharge rate at 75 mA g^{-1}.

specific impedance (ASI). The ASI is the ratio of voltage drop to current density during a charge or discharge pulse. Even though the value of the ASI may change as a function of many factors including pulse magnitude and duration, SOC, electrode thickness, etc. [37–40], it serves as a quick and simple means to estimate the impedance of the cell under given test conditions.

Fig. 5a and b compares the ASI of ANL-NMC to the blended electrode as a function of electrode potential for 3C discharge and charge pulses (2 mA cm^{-2} or ~0.45 A g^{-1}), respectively. The measured ASI was significantly lowered by incorporating the LFP into the electrode, particularly at low electrode potentials (or at low SOC).

The ANL-NMC material displays an interesting asymmetry in the ASI plot for discharge pulses. The charge pulse ASI displays a "V" shape over the range of cell voltages that may be derived from the expected behavior of the lithium diffusion in layered materials [12] although the exact structure of the ANL-NMC after activation is not understood well [5,6]. Conversely, the discharge ASI increases rapidly for cell potentials below 3.4 V. The reason for this behavior is not yet understood. The higher impedance for a discharge pulse compared to charge pulse at low SOC has been reported previously. Kang et al. [15] observed significantly slower kinetics during lithiation than delithiation at very low SOC ($Li_{1\pm\Delta}MO_2$, $\Delta \approx 0$) in their study of the first cycle irreversibility of lithium metal oxides. They hypothesized the formation of a Li_2MO_2 phase upon Li insertion into the highly lithiated layered oxide due to sluggish mass transport. The lower ASI on charge results from only the $LiMO_2$ phase being present. The Li_2MO_2 phase disappears during the open-circuit rest period as diffusion relaxes the concentration gradient before the charge current pulse. This phenomenon is certainly possible in the ANL-NMC material. Regardless, work in our laboratory has already produced other LMR-NMC materials exhibiting discharge ASI vs. SOC curves with less asymmetry. Lower impedance versions of these materials are under development by changing the stoichiometry and surface treatment. In addition, we note that the ANL-NMC cell here has relatively thin electrodes that result in an overall increase of the measured ASI [37–39]. A lower minimum ASI, ~60 Ω cm^2, has been measured for this material using a thicker electrode cell that would be more typical of an energy application. However this thickness dependence does not alter the slope of the increasing ASI at lower cell voltages.

The voltage behavior during and after discharge pulses beginning at different open-circuit cell voltages (V_0) is plotted in

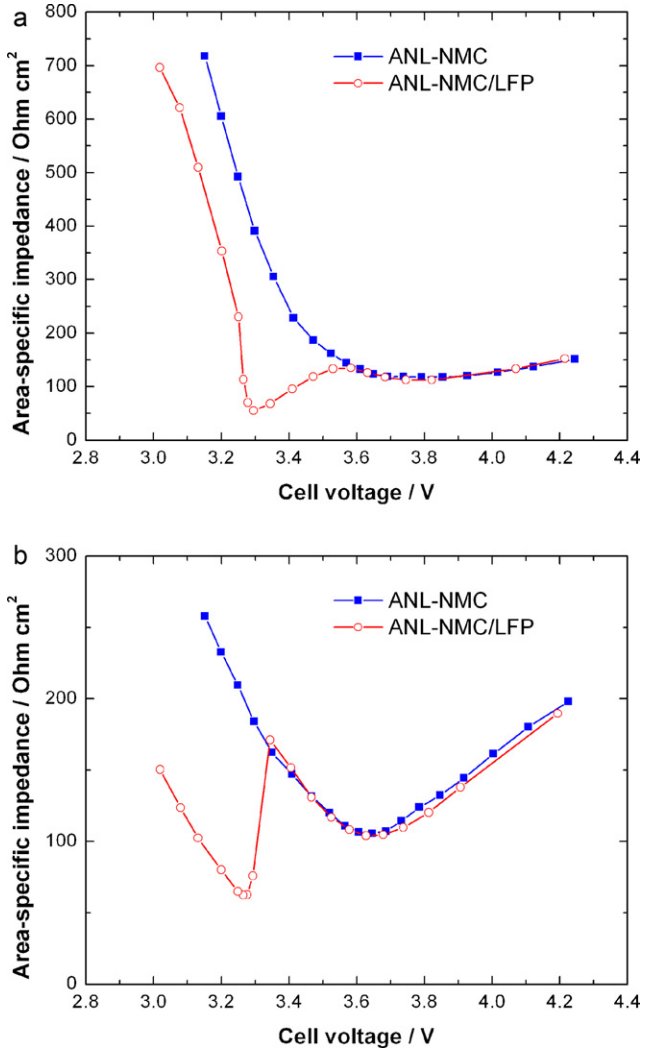

Fig. 5. (a) Discharge and (b) charge ASI as a function of cell voltage for 10-s 3C pulses.

Fig. 6. Electrochemical impedance spectroscopy utilizing a Li_ySn reference electrode determined the positive electrode to be the dominant source of the overall cell impedance [33]. The interaction between ANL-NMC and LFP particles is evident in the shape of the voltage curve during the pulse and the subsequent relaxation period at low V_0. Owing to its lower impedance, the LFP carriers the current demanded if the starting potential is low enough or the polarization of the electrode large enough.

The voltage trace starting at 3.58 V is typical of layered-oxide material and thus in a manner consistent with ANL-NMC. The initial drop in potential is due to polarization from ohmic and interfacial kinetic processes. The continuing decrease in potential during the current pulse results from the change in concentration of lithium at the surface of the oxide and the sloping open-circuit potential function of the ANL-NMC. After the 10-s pulse, the current was interrupted and the cell potential quickly increased in value as the kinetic and ohmic polarization was removed. However, the cell potential continues to relax as the concentration gradients force lithium transport within the electrodes and active particles themselves.

The interaction of LFP with ANL-NMC in the voltage response is found in the voltage traces beginning at open-circuit cell voltages of 3.47 and 3.41 V. The slope of the potential with time during the discharge pulse is in-between that expected for ANL-NMC and LFP alone. The LFP effect is more strikingly reflected in the

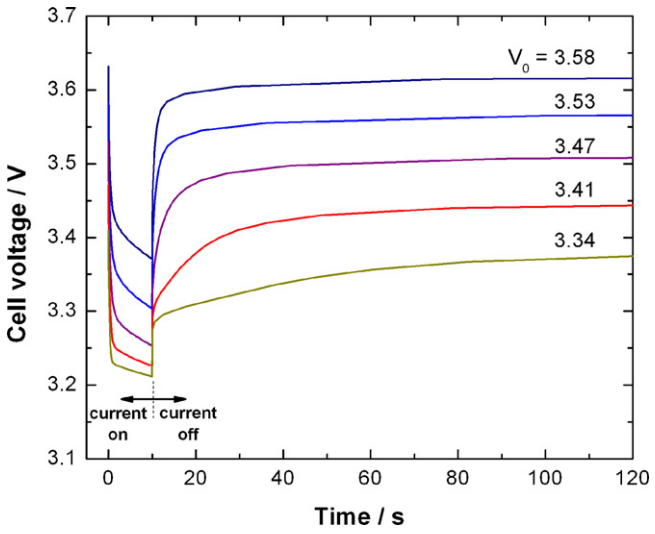

Fig. 6. 3C discharge pulses of ANL-NMC/LFP full cells from open-circuit voltages of 3.58, 3.53, 3.47, 3.41, and 3.34 V.

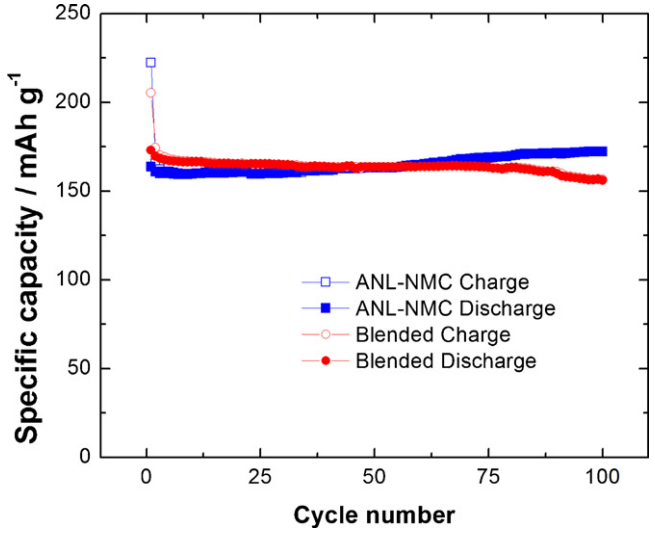

Fig. 7. Full cell cycling at C/1 rate, 2–4.5 V, C/10 cutoff at 4.5 V.

voltage relaxation curves after the current pulse is interrupted. Unlike the voltage relaxation curves for $V_0 \geq 3.47$, the relaxation for $V_0 = 3.41$ and 3.34 V seems to consist of two processes with different time constants, possibly the earlier relaxation process from LFP component in the electrode and the later one from ANL-NMC component.

Full Li-ion cell cycling results for 1C discharge and 1C charge with C/10 cutoff are shown in Fig. 7 after the two formation cycles. Both the ANL-NMC and blended electrode cells appear to have stable cycling under these conditions. Both cells display similar capacities, highlighting the negligible impact of blending from the lower energy LFP material. Future studies will optimize the electrode composition and more deeply evaluate lifetime performances. These studies will also evaluate the thermal stability of the blended electrode and hence project the safety of commercial systems. The thermal stability of ANL-NMC has been previously reported in Ref. [31] and various reports on delithiated LFP may be found, for example [41,42].

4. Conclusions

This work presents an example of using two materials to reach collective goals that neither could achieve on their own. A physical blend of ANL-NMC with LFP has been demonstrated as a path to lower the impedance of ANL-NMC materials at low SOC. The LFP acts as an internal low impedance pathway over $Fe^{2+/3+}$ active potential window, carrying the current for the more resistive ANL-NMC material. The ANL-NMC material used in this work has not yet reached a final state of development. Future materials will have enhanced rate capability and improved pulse-power impedance than the stoichiometry presented here-in. However, all layered oxide materials suffer from a decrease in the lithium diffusion coefficient as the concentration of intercalated lithium increases near the maximum. Therefore, blending of a lower impedance material that is electrochemically active in the appropriate voltage range will likely continue to be beneficial in the future.

Acknowledgments

Support for this work from the Office of Vehicle Technologies of the U.S. Department of Energy is gratefully acknowledged. The submitted manuscript has been created by UChicago Argonne, LLC, Operator of Argonne National Laboratory ("Argonne"). Argonne, a U.S. Department of Energy Office of Science laboratory, is operated under Contract No. DE-AC02-06CH11357. The U.S. Government retains for itself, and others acting on its behalf, a paid-up, nonexclusive, irrevocable worldwide license in said article to reproduce, prepare derivative works, distribute copies to the public, and perform publicly and display publicly, by or on behalf of the Government.

References

[1] J.-M. Tarascon, M. Armand, Nature 414 (2001) 359–367.
[2] M. Armand, J.-M. Tarascon, Nature 451 (2008) 652–657.
[3] D.J. Santini, K.G. Gallagher, P.A. Nelson, International Electric Vehicles Symposium EVS-25, Shenzhen, China, 2010.
[4] TIAX LLC, "Cost Assessment for Plug-In Hybrid Vehicles (SOW-4656)," Report to US DOE Office of Transportation Technology, October, 2007.
[5] S.-H. Kang, P. Kempgens, S. Greenbaum, A.J. Kropf, K. Amine, M.M. Thackeray, Journal of Materials Chemistry 17 (2007) 2069–2077.
[6] M.M. Thackeray, S.-H. Kang, C.S. Johnson, J.T. Vaughey, R. Benedek, S.A. Hackney, Journal of Materials Chemistry 17 (2007) 3112–3125.
[7] Z. Lu, D.D. MacNeil, J.R. Dahn, Electrochemical and Solid-State Letters 4 (2001) A191–A194.
[8] H. Deng, I. Belharouak, R.E. Cook, H. Wu, Y.-K. Sun, K. Amine, Journal of the Electrochemical Society 157 (2010) A447–A452.
[9] S.-H. Kang, M.M. Thackeray, Electrochemistry Communications 11 (2009) 748–751.
[10] S. Kumar, Presented at the 27th International Battery Seminar & Exhibit, Fort Lauderdale, FL, March 14–18, 2010.
[11] Q.Y. Wang, J. Liu, V. Murugan, A. Manthiram, Journal of Materials Chemistry 19 (2009) 4965–4972.
[12] A. Van der Ven, G. Ceder, Journal of Power Sources 97–98 (2001) 529–531.
[13] K. Kang, G. Ceder, Physical Review B 74 (2006) 094105.
[14] S.-H. Kang, W.-S. Yoon, K.-W. Nam, X.-Q. Yang, D.P. Abraham, Reactivity of Solids 43 (2008) 4701–4706.
[15] S.-H. Kang, D.P. Abraham, W.-S. Yoon, K.-W. Nam, X.-Q. Yang, Electrochimica Acta 54 (2008) 684–689.
[16] J.W. Fergus, Journal of Power Sources 195 (2010) 939–954.
[17] T. Numata, Ch. Amemiya, T. Kumeuchi, M. Shirakata, M. Yonezawa, Journal of Power Sources 97–98 (2001) 358–360.
[18] A. Manthiram, W. Choi, Electrochemical and Solid-State Letters 10 (2007) A228–A231.
[19] N. Imachi, Y. Takano, H. Fujimoto, Y. Kida, S. Fujitani, Journal of the Electrochemical Society 154 (2007) A412–A416.
[20] J. Gao, A. Manthiram, Journal of Power Sources 191 (2009) 644–647.
[21] H. Gan, R.S. Rubino, E.S. Takeuchi, Journal of Power Sources 146 (2005) 101–106.
[22] J.F. Whitacre, K. Zaghib, W.C. West, B.V. Ratnakumar, Journal of Power Sources 177 (2008) 528–536.
[23] K.-W. Nam, W.-S. Yoon, H. Shin, K.-Y. Chung, S. Choi, X.-Q. Yang, Journal of Power Sources 192 (2009) 652–659.
[24] P. Albertus, J. Christensen, J. Newman, Journal of the Electrochemical Society 156 (2009) A606–A618.

[25] P.M. Gomadam, D.R. Merritt, E.R. Scott, C.L. Schmidt, P.M. Skarstad, J.W. Weidner, Journal of Power Sources 174 (2007) 872–876.
[26] The United States Environmental Protection Agency Dynamometer Driving Schedules http://www.epa.gov/nvfel/testing/dynamometer.htm (accessed 14.04.11).
[27] A.K. Padhi, K.S. Nanjundaswamy, J.B. Goodenough, Journal of the Electrochemical Society 144 (1997) 1188–1194.
[28] J.B. Goodenough, Journal of Power Sources 174 (2007) 996–1000.
[29] C.M. Julien, A. Mauger, A. Ait-Salah, M. Massot, F. Gendron, K. Zaghib, Ionics 13 (2007) 395–411.
[30] M.S. Whittingham, Chemical Reviews 104 (2004) 4271–4301.
[31] S.-H. Kang, K. Amine, Journal of Power Sources 146 (2005) 654–657.
[32] S.-H. Kang, C.S. Johnson, J.T. Vaughey, K. Amine, M.M. Thackeray, Journal of the Electrochemical Society 153 (2006) A1186–A1192.
[33] K.G. Gallagher, D. Kim, S.-H. Kang, The 218th Meeting of the Electrochemical Society, Las Vegas, NV, October 10–15, 2010.
[34] S.-H. Park, S.-H. Kang, I. Belharouak, Y.K. Sun, K. Amine, Journal of Power Sources 177 (2008) 177–183.
[35] C. Xu, J. Lee, A.S. Teja, Journal of Supercritical Fluids 44 (2008) 92–97.
[36] Y.-H Chen, C.-W. Want, G. Liu, X.-Y. Song, V.S. Battaglia, A.M. Sastry, Journal of the Electrochemical Society 154 (2007) A978–A986.
[37] K.G. Gallagher, P.A. Nelson, D.W. Dees, Journal of Power Sources 196 (2011) 2289–2297.
[38] D. Dees, E. Gunen, D. Abraham, A. Jansen, J. Prakash, Journal of Electrochemical Society 155 (2008) A603–A613.
[39] W. Lu, A. Jansen, D. Dees, P. Nelson, N.R. Veselka, G. Henriksen, Journal of Power Sources 196 (2011) 1537–1540.
[40] D.P. Abraham, D.W. Dees, J. Christophersen, C. Ho, A.N. Jansen, International Journal of Energy Research 34 (2010) 190–203.
[41] J. Jiang, J.R. Dahn, Electrochemical Communications 6 (2004) 724.
[42] H.F. Xiang, H. Wang, X.W. Ge, S. Guo, J.H. Sun, W.Q. Hu, Journal of Power Sources 191 (2009) 575–581.